Journal of Ceramic Processing Research. Vol. 17, No. 5, pp. 499~503 (2016)

J O U R N A L O F
Ceramic Processing Research

Crystallization kinetics and magnetic properties of spinel transition metal ferrite nanoparticles

Yukun Sun[a], Dongyun Li[a,*], Pengzhao Gao[b], Zhouli Lu[b] and Hongliang Ge[a]

[a]*College of Materials Science and Engineering, China Jiliang University, Hangzhou 310018, China*
[b]*College of Materials Science and Engineering, Hunan University, Changsha, 410082, China*

Spinel transition metal ferrite $TMFe_2O_4$ (TM = Co^{2+}, Ni^{2+}, Cu^{2+}, and Zn^{2+}) nanoparticles were prepared via a template-assisted sol-gel method followed by a calcining process, using metal nitrate precursors as raw materials. The prepared specimens were characterized using X-ray diffraction (XRD) and a vibrating sample magnetometer (VSM). Their structures, magnetic properties, crystallization kinetics, and the influence of crystal size (D) on the magnetic properties were investigated. It was found that the crystal sizes of $TMFe_2O_4$ were positively proportional to the calcined temperature and time, and the crystallization growth activation energy (E_a) increased with the increase of metal ionic radius. The optimum calcination parameters were obtained to form a crystal closest to the standard crystal. Additionally, the saturation magnetization of inverse spinel structure specimens was enhanced monotonously and their coercivity showed a potential decrease trend, while there was an opposite change trend for normal spinel structure specimens.

Key words: Transition metal ferrites, Crystallization kinetics, Magnetic properties, Nano particles.

Introduction

Spinel ferrite nanoparticles are one of the most important nano materials because of their significant electronic, optical, electrical, magnetic properties which are different from their bulk structure [1-6]. It is noted that the performance of ferrite nanoparticles, partly dependent on the synthesis method, is crucial for the performance of final devices [7-10]. Ferrite nanoparticles are usually prepared via the sol-gel method, the chemical co-precipitation method, the microwave refluxing method, the hydrothermal method and so on [3-11]. Generally, the magnetic nanoparticles obtained via a sol-gel method are of high dispersivity, high sintering activity and stoichiometric composition [12-15].

The magnetic properties of ferrites are greatly influenced by the crystal size [16-18], which in turn are influenced by crystallization behavior. Thus, it is essential study of the crystallization kinetics of ferrites, and there is little investigation about the crystallization kinetics of transition metal ferrite $TMFe_2O_4$ up to now. In this paper, the crystallization kinetics and the relationship between magnetic properties and the average crystal size (D) of $TMFe_2O_4$ (TM=Co^{2+}, Ni^{2+}, Cu^{2+}, Zn^{2+}) nanoparticles are investigated.

*Corresponding author:
Tel : +86-571-87676293
Fax: +86-571-28889526
E-mail: lidongyun@cjlu.edu.cn

Experimental Procedures

Preparation of transition metal ferrite $TMFe_2O_4$ nanoparticles

Transition metal ferrite $TMFe_2O_4$ (TM = Co^{2+}, Ni^{2+}, Cu^{2+}, Zn^{2+}) nanoparticles were prepared by a template-assisted sol-gel method [10, 15, 19-21]. Metal nitrates together with citric acid, ethanol, and ammonia solution were used to prepare the starting sol. Firstly, the metal nitrates were dissolved in ethanol in required molar ratios to prepare solution A, and citric acid was dissolved in ethanol in a separate vessel to produce Solution B. Secondly, solution B was added into solution A, keeping stirred for 4 hrs, and then the mixture was quantitatively titrated by an ammonia solution to a pH of 2. Thirdly, the obtained sol was stirred for 24 hrs, and then was absorbed by cotton fiber. Finally, the sol was dried in an oven at 353 K, and then the dry gel was calcined at 673-1273 k for 1-4 hrs, respectively.

Characterization

The phase composition of specimens was determined by a X-ray diffractometer (Bruker D8 Phaser) using nickel filtered Cu K_α radiation ($\lambda = 0.154$ nm). The hysteresis loops were measured by a vibrating sample magnetometer (LakeShore7407 VSM) with a maximum external field H_m (20000 Oe). The Curie temperature (T_c) was determined from the dependency of magnetic moment on temperature obtained also by using a VSM with an applied magnetic field of 1.5 T in the range of 323-1073K.

Results and discussion

Influence of calcination processing parameters on the average crystal size of $TMFe_2O_4$ nanoparticles

The XRD patterns of $CoFe_2O_4$ calcined at different temperatures for 1 hr, different $TMFe_2O_4$ nanoparticles calcined at 1073 K for 1h and $NiFe_2O_4$ calcined at 1073 K for 1-4 hrs with steps of 1 hr are given in Fig. 1(a-c), respectively. All the patterns are indexed to the typical spinel structure ($CoFe_2O_4$ corresponds to PDF#04-0787, $NiFe_2O_4$ to PDF#10-0325, $CuFe_2O_4$ to PDF#34-0425 and $ZnFe_2O_4$ to PDF#22-1012), suggesting all specimens are of the single phase structure.

Ferrites structural, magnetic and electrical properties depend on cation distribution in two sublattices. Magnetite is a spinel structure with the Fe^{3+} in the tetrahedral A-site and Fe^{3+} and Fe^{2+} in octahedral B-site [5-7, 10]. In the transition metal ferrites, $CoFe_2O_4$, $NiFe_2O_4$ and $CuFe_2O_4$ crystals have inverse spinel structure [22-23, 28-29], in which the tetrahedral A-sites are occupied by the Fe^{3+} ions, and the octahedral B-sites are occupied by the transition metal divalent cation and Fe^{3+}. But in $ZnFe_2O_4$, which has a normal spinel type, the A-sites are occupied by Zn^{2+} and B-sites are occupied by Fe^{3+} [3, 30].

The Scherrer equation [10] (Eq.1) is used to calculate the average crystal size (D) of $TMFe_2O_4$ specimens.

$$D = \frac{0.89\lambda}{B\cos\theta} \quad (1)$$

Where, B is the peak width at half-height, and λ is the wavelength of X-ray. The D of $TMFe_2O_4$ nanoparticles calculated according to equation (1) is shown in Fig. 2. It can be seen that average crystal size (D) of $TMFe_2O_4$ is positively proportional to the calcined time and temperature, and that the effect of the calcined temperature is more obvious than that of the calcined time.

Crystallization kinetics of $TMFe_2O_4$ nanoparticles

The relationships of average crystal size (D) and the calcination time for different $TMFe_2O_4$ nanoparticles are shown in Fig. 2. The slope K and correlation coefficient r of each curve in Fig. 2 are listed in Table 1. As is described above, the average crystal size

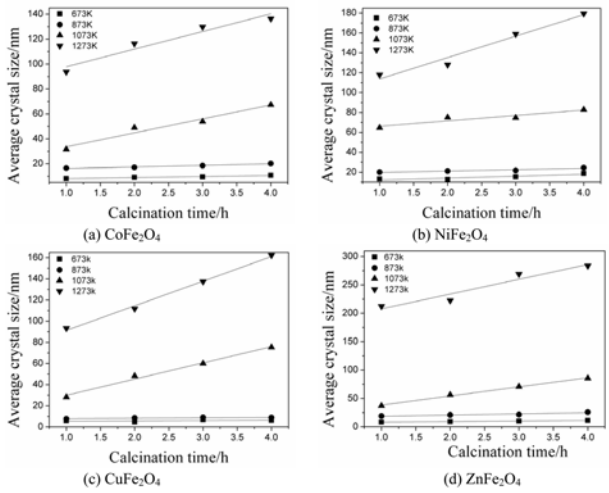

Fig. 2. Dependency of average crystal size on the calcination time for different specimens.

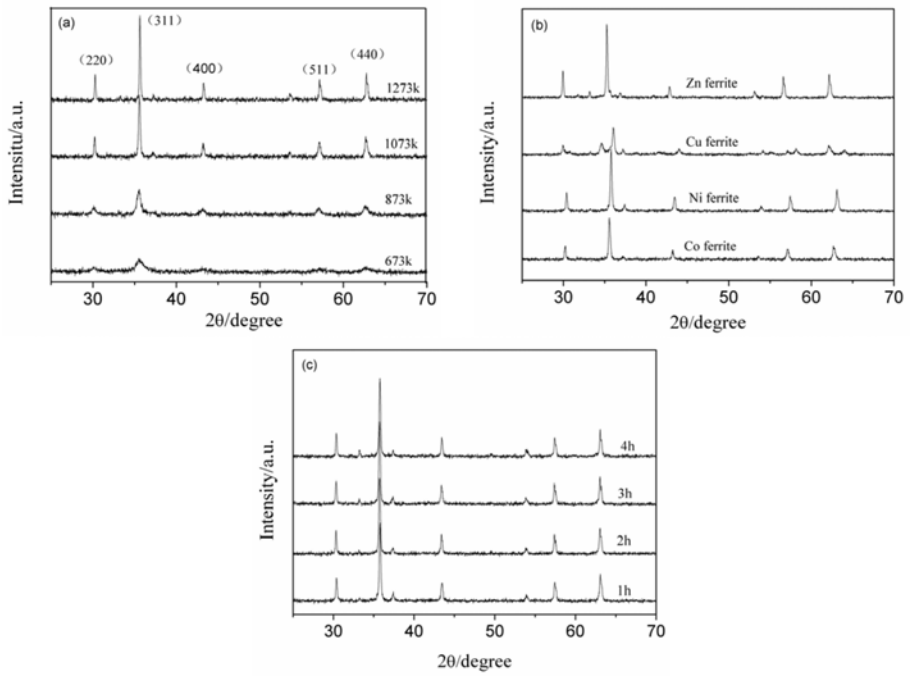

Fig. 1. XRD patterns of different specimens (a) $CoFe_2O_4$ calcinated at different temperatures for 1 hr; (b) Different $TMFe_2O_4$ calcined at 1073 K for 1 hr; (c) $NiFe_2O_4$ calcined at 1073 K for different times.

Table 1. The slopes (*K,* nm/k) and correlation coefficients(*r*) of each curve shown in Fig. 2.

Specimens	673K		873K		1073K		1273K	
	K	r	K	r	K	r	K	r
CoFe2O4	0.85	0.946	1.22	0.947	11.2	0.941	14.13	0.908
NiFe2O4	1.95	0.933	1.34	0.845	5.42	0.818	21.54	0.953
CuFe2O4	0.35	0.977	0.41	0.959	15.31	0.984	23.27	0.992
$ZnFe_2O_4$	1.02	0.986	2.1	0.837	16.01	0.992	26.02	0.900

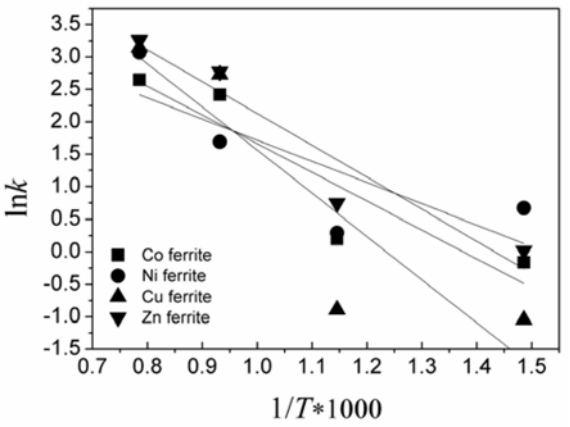

Fig. 3. The relationship between ln*k* and 1/*T* for $TMFe_2O_4$ nanoparticles.

(*D*) is proportional to the calcined time for each calcined temperature. Thus, the activation energy E_a for the crystal growth of $TMFe_2O_4$ nanoparticles could be calculated from the calcined time and temperature dependence of the rate of crystallization which can be obtained from the crystallization curve using Arrhenius equation [25-27],

$$\ln k = \ln A - \frac{E_a}{RT} \quad (2)$$

Table 2. Valence electron structure, ionic radius and activation energy of transition metals.

Metal element	Co	Ni	Cu	Zn
Valence electron structure	$3d^74s^2$	$3d^84s^2$	$3d^{10}4s^1$	$3d^{10}4s^2$
Ionic radius/nm	0.074	0.069	0.082	0.083
E_a/(kJ·mol^{-1})	36.78	27.13	55.24	40.83

Where *k* is the rate of crystallization, *A* is pre-exponential factor, *T* is the absolute temperature in *K*, and *R* is the gas constant in J·mol^{-1}·K^{-1}. In the experimental conditions, ln*A* was constant. The Arrhenius curve would be obtained through plotting ln*k* versus *1/T* (the data of *k* and *T* can be obtained from Fig. 2), which are plotted in Fig. 3, and the values of E_a can be obtained from the slopes of these curves.

Valence electron structure, ionic radius and activation energy of several transition metals are listed in Table 2 [28-32]. As can be concluded from Table 2, the E_a increases with larger transition metal ionic radius for the spinel specimens crystal growth, which could be attributed to that the larger ion needs more energy to enter into the spinel lattice. Particularly, it would need higher E_a for crystal growth of $CuFe_2O_4$ because of its tetragonal distortion explained by John-Teller effect [22-24].

Table 3. Cell parameters of different $TMFe_2O_4$ obtained by the XRD Rietveld refinement method.

Specimens		a, b, c/Å				Standard materials a, b, c /Å
		1 h	2 h	3 h	4 h	
$CoFe_2O_4$ (a=b=c;α=β=γ=90 °)	673K	8.8065	8.9934	8.0873	7.9382	8.377
	873K	8.3854	8.3732	8.3729	8.3636	
	1073K	8.321	8.257	8.4427	8.3922	
	1273K	8.3528	8.3607	8.3507	8.3593	
$NiFe_2O_4$ (a=b=c;α=β=γ=90 °)	673K	8.3309	8.3148	8.3574	8.3051	8.339
	873K	8.3266	8.3179	8.3215	8.3298	
	1073K	8.3037	8.3341	8.3117	8.3291	
	1273K	8.3311	8.3263	8.3367	8.3852	
$CuFe_2O_4$ (a=b=c;α=β=γ=90 °)	673K	5.6275, 8.3271	5.8470, 8.5801	5.8412, 8.6425	5.8441,8.5631	5.8444,8.6304
	873K	5.8024, 8.5782	5.8580, 8.6326	5.7695, 8.6285	5.8287, 8.6313	
	1073K	5.8175, 8.6646	5.8280, 8.6984	5.8424, 8.6314	5.8137, 8.7042	
	1273K	5.7354, 8.8650	5.8107, 8.6505	5.8130, 8.5612	5.8242, 8.6622	
$ZnFe_2O_4$ (a=b=c;α=β=γ=90 °)	673K	8.4275	8.3928	8.4448	8.4451	8.4411
	873K	8.4148	8.4307	8.4096	8.4137	
	1073K	8.4543	8.4045	8.4247	8.4520	
	1273K	8.4735	8.4562	8.4549	8.6652	

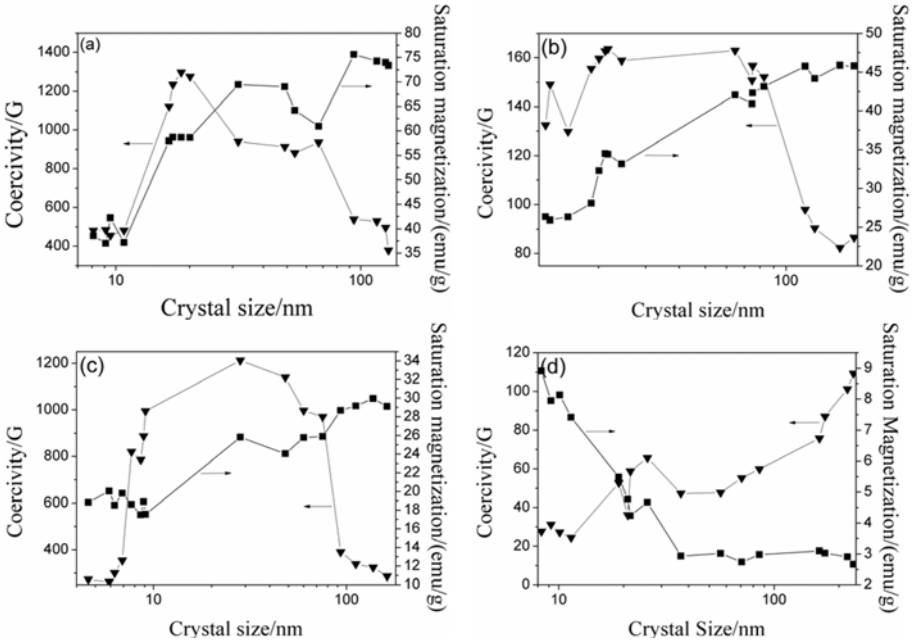

Fig. 4. The relationship between the magnetic properties and the crystal size for different $TMFe_2O_4$ specimens (a) $CoFe_2O_4$; (b) $NiFe_2O_4$; (c) $CuFe_2O_4$ and (d) $ZnFe_2O_4$.

Influence of the calcination processing parameters on the cell parameters of $TMFe_2O_4$ nanoparticles

The cell parameters for $TMFe_2O_4$ obtained by XRD Rietveld refinement are listed in Table 3. The standard cell parameters for $CuFe_2O_4$ are 5.8444Å (a) and 8.6304 Å (c), and that was 8.377 Å, 8.339 Å and 8.4411 Å for $CoFe_2O_4$, $NiFe_2O_4$ and $ZnFe_2O_4$, respectively. As can be seen from Table 3, the cell parameters are very close to the standard data. Compared with the standard data, to prepare a crystal similar to the standard material, the best calcined processing parameters should be 1273K-3 hrs, 1273K-3 hrs, 1073K-2 hrs and 1073K-1 hr for $CoFe_2O_4$, $NiFe_2O_4$, $CuFe_2O_4$ and $ZnFe_2O_4$, respectively.

Influence of crystal size on the magnetic properties of $TMFe_2O_4$ nanoparticles

The dependency of magnetic properties on the crystal size of $TMFe_2O_4$ specimens is shown in Fig. 4. It is revealed that, for inverse spinel specimens, the M_s increased monotonously, and the coercivity (H_c) increased first and then decreased, while the M_s decreased and H_c increased for normal spinel structure ($ZnFe_2O_4$) with the increasing of crystal size. For hard magnetic $CoFe_2O_4$ and $CuFe_2O_4$, the highest H_c of about 1200 ± 100 Oe and 1100 ± 100 Oe can be obtained when the crystal size (D) is controlled to be 30-70 nm and 15-25 nm, respectively, and the lowest is 80 ± 10 Oe for $NiFe_2O_4$. The highest M_s of about 70 ± 5emu/g, 45 ± 1 emu/g and 29 ± 1 emu/g are observed for $CoFe_2O_4$, $NiFe_2O_4$ and $CuFe_2O_4$, respectively.

The domain of magnetic nanoparticles would be collapsed and the ordered structure turns to be disordered when the temperature exceeds the Curie temperature (T_c). The relationship of T_c and the crystal size (D) for $TMFe_2O_4$ calcined for 1h are shown in Fig. 5. The Curie temperature increases from 828 K to 853 K and from 773 K to 838 K for $NiFe_2O_4$ and $ZnFe_2O_4$ ferrites, respectively, as the crystal size (D) increases. The maximum of the Curie temperature for $CoFe_2O_4$ ferrites is 810 K when the crystal size (D) is in the range of 30-70 nm. The crystal size (D) has no obvious influence on T_c of $CuFe_2O_4$ for its unique cell structure [22-24].

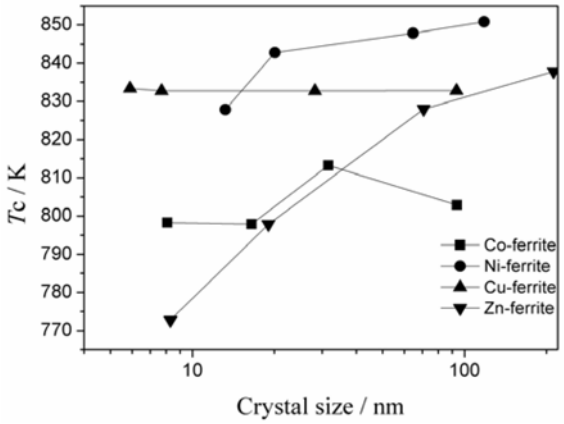

Fig. 5. The relationship of the Curie temperature *T*c and the crystal size for different $TMFe_2O_4$ nanoparticles calcined for 1 hr.

Conclusions

$TMFe_2O_4$ nanoparticles were prepared by template-assisted sol-gel method. The crystallization kinetics and magnetic properties of $TMFe_2O_4$ are studied. The average crystal size of spinel specimens is positively proportional to the calcined temperature and the holding time, and the

activation energy is enhanced with the increasing the transition metal ionic radius. As can be seen from the refinement of XRD data, the optimum calcined conditions are 1273K-3 hrs, 1273K-3 hrs, 1073K-2 hrs and 1073K-1 hr for $CoFe_2O_4$, $NiFe_2O_4$, $CuFe_2O_4$ and $ZnFe_2O_4$, respectively, to prepare a crystal similar to the standard materials. The results of magnetic properties measured by VSM reveal that the M_s of inverse spinel specimens is enhanced monotonously and the coercivity shows a potential decrease trend, while it shows an opposite change trend for normal spinel structure. The Curie temperature increases from 828 K to 853 K and from 773 K to 838 K for $NiFe_2O_4$ and $ZnFe_2O_4$, respectively, as the crystal size increases. The highest Curie temperature of $CoFe_2O_4$ is 810 K obtained with the crystal size of 30-70 nm. The Magnetic properties of $CuFe_2O_4$ show abnormal change because of its distorted structure.

References

1. A. Rana, O.P. Thakur, V. Kumar, Mater. Lett. 65 (2011) 3191-3192.
2. Z. Karimi, L. Karimi, H. Shokrollahi, Mater. Sci. Eng. C 33 (2013) 2465-2475.
3. N.M. Deraz, A. Alarifi, Int. J. Electrochem. Sci. 7 (2012) 5828-5836.
4. U.B. Sontu, V. Yelasani, V. Ramana R. Musugu, J. Magn. Magn. Mater. 374 (2015) 376-380.
5. A.N. Birgani, M. Niyaifar, A. Hasanpour, J. Magn. Magn. Mater. 374 (2015) 179-181.
6. Z.K. Karakaş, R. Boncukcuoğlu, İ.H. Karakaş, Magn. Magn. Mater. 374 (2015) 298-306.
7. D. Li, X. Hu, Y. Sun, S. Su, A. Xia, H. Ge, RSC Adv. 5 (2015) 27091-27096.
8. B.S. Randhawa, H.S. Dosanjh, M. Kaur, Ceram. Int. 35 (2009) 1045-1049.
9. P.M.P. Swamy, S. Basavaraja, A. Lagashetty, et al, Indian Acad. Sci. 34[7] (2011) 1325-1330.
10. P. Gao, X. Hua, V. Degirmenci, et al, J. Magn. Magn. Mater. 348 (2013) 44-50.
11. A. Xia, S. Liu, C. Jin, L. Chen, Y. Lv, Mater. Lett. 105 (2013) 199-201.
12. T. Li, Y. Li, R. Wu, H. Zhou, X. Fang, S. Su, A. Xia, C. Jin, X. Liu, J. Magn. Magn. Mater. 393 (2015) 325-330.
13. A.V. Raut, R.S. Barkule, D.R. Shengule, et al, J. Magn. Magn. Mater. 358-359 (2014) 87-92.
14. M. Sajjia, M. Oubaha, M. Hasanuzzaman, A.G. Olabi, Ceram. Int. 40 (2014) 1147-1154.
15. D.-Y. Li, Y.-K. Sun, P.-Z. Gao, et al, Ceram. Int. 40 (2014) 16529-16534.
16. C.A. Stergiou, V. Zaspalis, Ceram. Int. 40 (2014) 357-366.
17. X. Kong, M. Zhu, J. Zheng, Trans. Mater. Heat Treat. 25[5] (2004) 288-290.
18. A. Xia, C. Zuo, L. Zhang, C. Cao, Y. Deng, W. Xu, M. Xie, S. Ran, C. Jin, X. Liu, Journal of Physics D: Applied Physics. 47 (2014) 415004.
19. J. Liu, P. Liu, X. Zhang, Ultrason. Sonochem. 23 (2015) 46-52.
20. E.V. Rebrov, P. Gao, et al, Magn. Mater. 323 (2011) 723-729.
21. H. Arabi, F. Ganjali, J. Superconduct. Nov. Magn. 26 (4) (2013) 1031-1035.
22. S. Kimura, T. Mashino, T. Hiroki, et al, Thermochim. Acta 532 (2012) 119-122.
23. S. Manjura Hoque, M. Samir Ullah, F.A. Khan, et al, Phys. B 406 (2011) 1799-1804.
24. A. Azam, J. Alloys Comp. 540 (2012) 145-153.
25. J.L. Cardenas-Leal, J. Vazquez, P.L. Lopez-Alemany, et al, J. Alloys Comp. 471 (2009) 44-51.
26. P.S. Niphadkar, N.P. Tangale, P.N. Joshi, et al, Microporous Mesoporous Mater. 182 (2013) 73-80.
27. C. Rodríguez-Tinoco, M. Gonzalez-Silveira, J. Ràfols-Ribé, et al, J. Non-Cryst. Solids 407 (2015) 256-261.
28. K. Kamala Bharathi, C.V. Ramana, Cambridge J. 26[4] (2011) 584-591.
29. A.M. Dumitrescu, A.I. Borhan, A.R. Iordan, et al, Powder Technol. 268 (2014) 95-101.
30. B.R. Reddy, T. Sivasankar, M. Sivakumar, et al, Ultrason. Sonochem. 17 (2010) 416-426.
31. A. Moser, Polyhedron 20 [15] (2001) 1897-1901.
32. S.T. Breviglieri, É.T.G.C., G.O. Chierice, Thermochim. Acta 356[1-2] (2000) 79-84.